Optical Materials 112 (2021) 110757

Contents lists available at ScienceDirect

Optical Materials

journal homepage: http://www.elsevier.com/locate/optmat

Research Article

Ta_2O_5 reinforced Bi_2O_3–TeO_2–ZnO glasses: Fabrication, physical, structural characterization, and radiation shielding efficacy

Gokhan Kilic [a], F.I.El Agawany [b,*], Buse Ozen Ilik [c], K.A. Mahmoud [d,e], Erkan Ilik [a], Y. S. Rammah [b]

[a] Eskisehir Osmangazi University, Faculty of Science and Letters, Department of Physics, TR 26040, Eskisehir, Turkey
[b] Department of Physics, Faculty of Science, Menoufia University, Shebin El-Koom, 32511, Menoufia, Egypt
[c] General Directorate of Mineral Research and Exploration, Ankara, Turkey
[d] Ural Federal University, 19 Mira St, 620002, Yekaterinburg, Russia
[e] Nuclear Materials Authority, P. O. Box 530, El Maadi, Cairo, Egypt

ARTICLE INFO

Keywords:
Bismuth tellurite glasses
Ta_2O_5
Raman
Deconvolution
Transmission factor

ABSTRACT

The melt-quenching method was applied to fabricate a new glass series containing $10Bi_2O_3$–$70TeO_2$-(20-x)ZnO-xTa_2O_5, x = 0, 2, 4, and 6 mol%. The chemical compounds were well mixed and melted in a furnace at 900 °C, and then the molten transferred to another furnace at 320 °C for annealing. X-ray diffraction is used to confirm the amorphous phase of the fabricated glasses. Moreover, the fabricated glasses' structure characterization was established using Raman analyses. Besides, the gamma-ray protection capacity was evaluated for the fabricated glass series. Thus, the MCNP-5 simulation code and XCOM software program were utilized to estimate the investigated glass samples' linear attenuation coefficients. The glass sample's highest attenuation coefficient, with 6 mol % of the Ta_2O_5 doping ratio is ranged between 418.17 and 0.27 cm^{-1}. In comparison, the fabricated glass without Ta_2O_5 possesses the lowest attenuation factor and decreased from 359.39 cm^{-1} to 0.26 cm^{-1}, raising the incoming photon energy from 0.015 MeV to 15 MeV, respectively. The simulated linear attenuation coefficient was then applied to calculate the half-value thickness, and transmission factor for the incoming photons. The obtained results showed that the fabricated glass samples' shielding ability enhanced with the insertion of the Ta_2O_5.

1. Introduction

Tellurium oxide (TeO_2) based glasses are among the glass structures studied most frequently due to their higher densities and melting at lower temperatures than boron glasses with high mechanical endurance [1–3]. Tellurite glasses, known as conditional glass formers, constitute durable amorphous glass structures when their appropriate synthesis and annealing temperatures are determined [4,5]. While basic glass compositions of tellurite glasses having high chemical durability and mechanical endurance are being prepared [6]. It is known that tellurite glasses doped with transition metal elements, especially ZnO, exhibit semiconducting character [7–12]. On the other hand, though zinc-tellurite glasses have higher densities and refractive indices, they are softer than silicate glasses mechanically [13]. In addition to necessary characterization studies in which physical, structural, optical, and thermal properties of zinc-tellurite glasses were found in the literature [14,15], ternary glass compositions of the same structure were synthesized and examined, as well [16,17].

Since oxide glasses doped with PbO, which is among the heavy metal oxides, pose a threat both to living beings and the environment, heavy metal oxides such as Bi_2O_3 can be used in tellurite glasses alternatively [18]. Since bismuth oxide (Bi_2O_3) has a low melting temperature, just like tellurium oxide, it is used in glass synthesis instead of toxic heavy metals. Glasses containing Bi_2O_3 can be used for protection from radiation by this means. It is known that glass structures such as bismuth borate [19], bismuth silicate [20], bismuth germanate [21] are also found in the literature in addition to bismuth oxide doped zinc-tellurite glasses.

Ta_2O_5 doped glasses with high refractive indices are being used in optics and the production of ceramic capacitors and piezoelectric ceramics [22]. In addition to the synthesis of Ta_2O_5 doped glasses with the classical melt-quenching method, studies in which they are formed with

* Corresponding author.
E-mail address: fouaadesmael@yahoo.com (F.I.El Agawany).

https://doi.org/10.1016/j.optmat.2020.110757
Received 11 November 2020; Received in revised form 11 December 2020; Accepted 16 December 2020
Available online 31 December 2020
0925-3467/© 2020 Elsevier B.V. All rights reserved.

different techniques to contain pure or more than one chemical are also present in the literature [22,23]. Besides, these studies are considered to have an essential role in photonic applications [24]. On the other hand, zinc-tellurite glasses doped with Ta_2O_5 were examined in our previous studies in detail [4,25,26].

In the field of gamma and neutron ionizing radiation protection, glasses and glass-ceramics have been used widely used as radiation shielding [27–31]. The capacity of using these materials as radiation shielding mainly depends on evaluating several shielding parameters such as linear/mass attenuation coefficients (MLAC/MAC), mean free path (MFP), half-value layer (HVL), and effective atomic number (Z_{eff}) [27–31].

In this study, since physical, structural, and especially radiation shielding properties contribute to the change in the properties, unlike previous studies, Bi_2O_3 and Ta_2O_5 at a specific ratio were added to TeO_2–ZnO binary glass structure having relatively high density. Thus, the synthesized glasses' densities and the molar volume were increased, and variations on the structural properties were aimed.

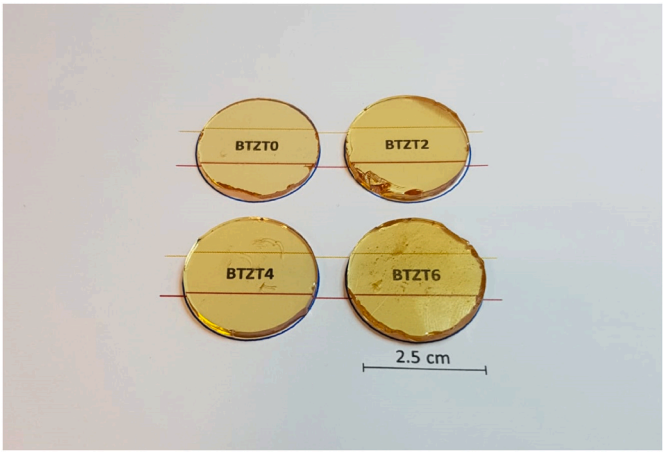


Fig. 1. Photograph of BTZT samples.

2. Experimental and calculations

2.1. Experimental procedure

The present synthesized glass composition was determined by the formula $10Bi_2O_3{\cdot}70TeO_2{\cdot}(20\text{-}x)ZnO{\cdot}xTa_2O_5$ (x = 0, 2, 4, 6 mol%). Oxide compounds with high purity (Alfa Aesar 99.5%) were weighed with an analytical balance (KERN ABT 100-5 M with a sensitivity of 0.00001) and mixed in a sterile sample vessel period mechanically. The classical melt-quenching method was preferred in the synthesis of glass samples. The prepared mixture was transferred to a platinum crucible and then placed in a high-temperature furnace (Nabertherm P310) previously heated to 900 °C and kept inside for 30 min, allows the reaction between melted compounds to take place. During this period, the crucible was removed from the furnace at certain intervals, and the molten mixture was stirred. The steel mold where the molten mixture would be poured into was placed in a second annealing furnace, and the temperature was set to a constant 320 °C. When the synthesis is complete, the mold preheated in the annealing furnace and the mixture melted in the high-temperature furnace were taken out simultaneously. The process of casting into steel mold was performed. The sample was kept in the annealing furnace at 320 °C for 60 min and then left to cool to room temperature. Shaping processes of the glasses that have been removed from the mold at room temperature before characterization was performed with Metkon Micracut 151 and Metkon Forcipol 1V grinder-polisher device. Codes of the synthesized samples, glass compositions, and physical properties belonging to these compositions are listed in Table 1, and images of these successfully synthesized glasses are presented in Fig. 1.

In the characterization of glasses, firstly, physical properties such as density, molar volume were determined. For the synthesized samples' structural properties, XRD analyses were established using (Bruker D8 Advance device between 10 and 90° at 0.01-degree steps and 18.8 s step time at 25 °C room temperature). Then Raman analyses and the glass structure's general characterization were performed utilizing (Renishaw Invia Raman microscope spectrometer having a resolution of 4 cm^{-1} and excitation of 532 nm between the range of 100–1000 cm^{-1}). Peak examinations of the XRD spectra were performed with the help of the High Score Plus program.

2.2. Photon shielding competences calculations

According to Beer-Lambert law, the exponential shielding law is given as [27,31]:

$$I = I_o e^{\mu x} \tag{1}$$

here, x and μ refer to the thickness and the linear attenuation coefficient. I and I_o refer to the transmitted and incident photon beams, respectively.

Moreover, the MAC values of the materials (glasses in the present study) and their essential elements have been performed utilizing XCOM as [27–31]:

$$MAC = \mu_\rho = \sum_i W_i \left(\frac{\mu}{\rho}\right)_i \tag{2}$$

here, w_i is the weight fraction of the ith essential element possessing the mass attenuation coefficient $(MAC)_i$.

In terms of the LAC values, the corresponding shielding parameter named half-value layer (HVL) can be calculated as the following relations, more detail in Refs. [27–31]. The HVL of the shielding material describes the thickness required to reduce the incident flux intensity to half of its initial value:

$$HVL = 0.693 \times \mu^{-1} \tag{3}$$

3. Results and discussion

3.1. Physical characterization

Density [32] and molar volume [33] values were calculated for each synthesized sample by using the Archimedes principle (Table 1). According to this, it can be clearly seen that the glasses' density values vary between 6.216 g cm^{-3} and 6.465 g cm^{-3}. The measured density was observed to increase almost linearly with the addition of Ta_2O_5 (Fig. 2).

Table 1
Sample code, chemical composition, and Wt. fraction of elements for $70TeO_2$–$10Bi_2O_3$-(20-x) ZnO-xTa_2O_5 glasses.

Sample code	The weight fraction in mol %				Fractional abundance of elements in each sample (wt.%)					Density g/cm^3 ± 0.01	Molar Volume
	TeO_2	Bi_2O_3	ZnO	Ta_2O_5	O	Zn	Te	Ta	Bi		(cm^{-3} mol^{-1})
BTZT0	80	10	10	0	0.175419	0.035847	0.559607	0.0	0.229128	6.216	28.0875
BTZT 2	80	10	8	2	0.174167	0.065503	0.497141	0.030558	0.232631	6.287	28.9172
BTZT 4	80	10	6	4	0.174373	0.055346	0.472564	0.076587	0.221130	6.357	29.7329
BTZT 6	80	10	4	6	0.174488	0.046649	0.455199	0.110659	0.213005	6.465	30.3516

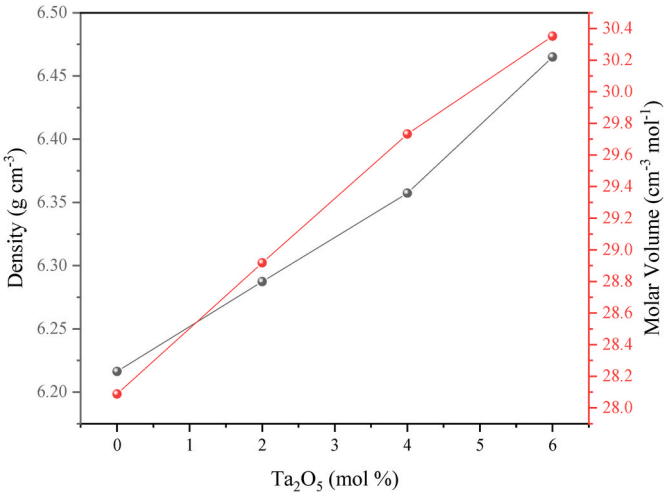


Fig. 2. Calculated densities and molar volume values of BTZT glasses.

Density increase occurred due to the substitution of ZnO with Ta_2O_5 in the structure. Besides, the Bi^{3+} atoms are believed to form non-bridging oxygen (NBO) in the glass network and change the glass structure [34]. When molecular weights are considered, this increase might be deemed to be observed since the molecular weight of ZnO was smaller than Ta_2O_5 (M_w (Ta_2O_5) = 441.893 g mol^{-1} > M_w (ZnO) = 81.38 g mol^{-1}). The calculated molar volume (V_M) varies between 28.0875 and 30.3516 cm^{-3} mol^{-1}. The calculated V_M value was observed to increase with raising the amount of Ta_2O_5 addition. It can be said that the glass network expands with a growth in the doping ratio. The obtained results were seen to be compatible with the literature [34,35].

3.2. Structural characterization

XRD spectra of synthesized BTZT samples are given in Fig. 3. In the 20–40° region of the spectrum, a wide-band having a peak point around 28° and revealing the amorphous structure of tellurite glasses is seen. Also, a second wide-band having a lower intensity is found around 50°.

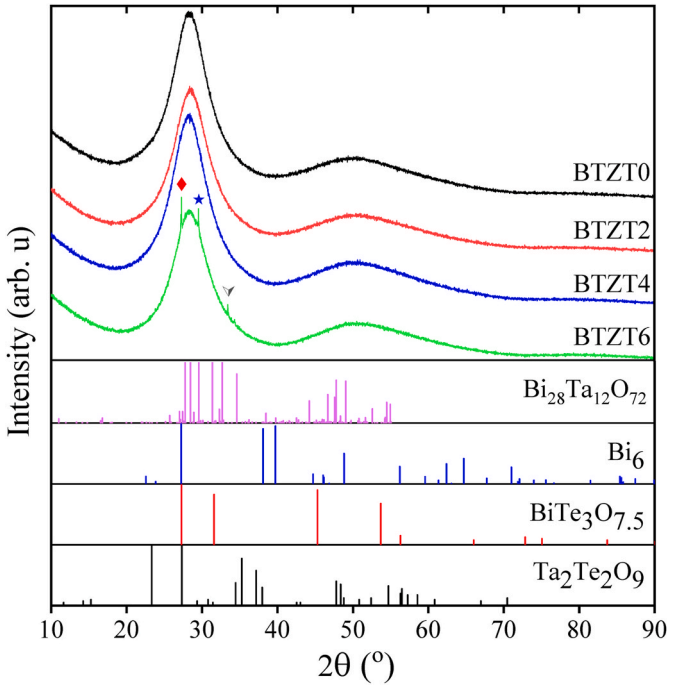


Fig. 3. XRD spectra of BTZT glasses.

This wide-band seen in XRD spectra obtained from the glasses synthesized in this study is relatively more intense than the bands observed in this region seen in TeO_2–ZnO containing glasses found in the literature [4]. As shown in Fig. 3, Bi and Ta containing compounds have characteristic bands observed intensely in this region. Therefore, it is natural for the wide-band seen in this region to have high intensity. Crystal peak was not encountered in samples that do not contain Ta_2O_5 and also contain 2% and 4% mol Ta_2O_5. It can be said that long-range crystal formation does not occur in these structures. On the other hand, when the spectrum belonging to the BTZT6 sample is examined, unlike other samples, three crystal peaks having low intensity attract attention when doping with Ta_2O_5 reaches the maximum amount. Among the 3 peaks detected, the first one at 27.30° is thought to belong to one of the $Bi_{28}Ta_{12}O_{72}$ (Ref. Code: 96-200-3078, bismuth tantalum oxide), Bi_6 (Ref. Code: 96-500-0216, bismuth), $BiTe_3O_{7.5}$ (Ref. Code: 00-049-1759, bismuth tellurium oxide), $Ta_2Te_2O_9$ (Ref. Code: 00-046-0956, tantalum tellurium oxide) compounds. It is highly probable that the two observed peaks around 29.52° and 33.43° belong to $Bi_{28}Ta_{12}O_{72}$; this also supports the opinion that the peak at 27.30 might be due to this compound well. By having Ta_2O_5 at the maximum molar ratio in the structure, we can conclude that Bi and Ta atoms combine with O and produce a bismuth tantalum oxide crystal structure.

Raman spectra of the synthesized glasses are given in Fig. 4. Raman spectra were obtained from the region of 100–4000 cm^{-1}, and eight Gaussian bands were obtained with the deconvolution process (with R^2 > 0.999 fitting parameters) of the 100-1100 cm^{-1} region of the obtained spectra (Table 2 and Fig. 5). As can be seen, an OH bond was not observed in the range of 1000–4000 cm^{-1}.

The spectra examination showed that the peaks observed between 116-118 cm^{-1} and 141-143 cm^{-1} (#1 and #2) belong to the characteristic γ- TeO_2 structure [26].

The Gaussian bands were observed in the range between 302 and 366 cm^{-1} (#3) to increase with Ta_2O_5 doping. The obtained results were compatible with those obtained by Mendoza et al. [36]. They reported that the Gaussian band was found in the same region for a Ta_2O_5 nanostructure. The band located in this region was seen to belong to bending vibrations of Ta–O–Ta. However, this band was estimated to belong to Ta–O–Ta due to the area increases with an increase in Ta_2O_5 content. For the BTZT0 sample not doped with Ta2O5, the band found within this range might be considered to be three unique Bi–O stretches or the β-Bi_2O_3 (tetragonal) phase, as well [37].

According to composition, Gaussian bands found in the range of

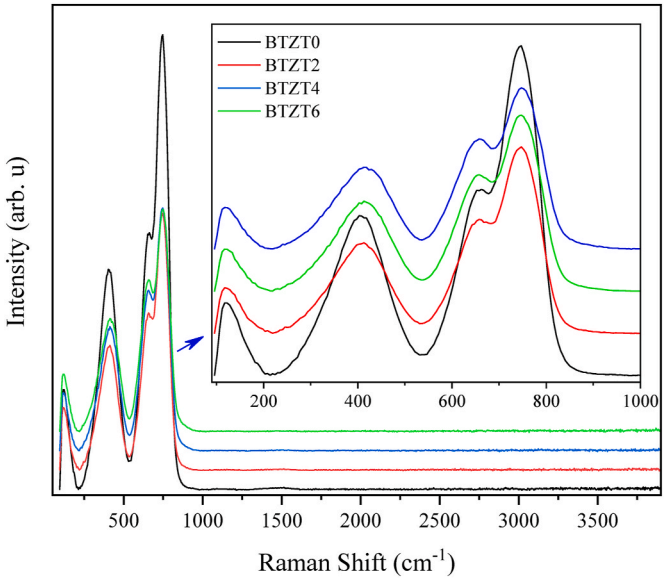


Fig. 4. Raman spectra of BTZT glasses.

Table 2
Peak values (C) and area percentages (A) of Raman spectra deconvolutions of BTZT glasses.

#	BTZT0		BTZT2		BTZT4		BTZT6	
	C (cm^{-1})	A %	C (cm^{-1})	A %	C (cm^{-1})	A %	C (cm^{-1})	A %
1	118	1.648	117	1.705	118	1.880	116	1.739
2	143	3.684	141	3.923	143	3.160	141	3.654
3	302	1.591	319	4.133	329	5.575	366	13.560
4	406	29.549	413	26.092	419	25.068	434	16.529
5	661	31.016	659	31.074	658	32.237	657	32.408
6	727	8.850	729	9.645	729	7.905	734	10.755
7	764	22.070	766	22.006	767	22.412	772	19.768
8	812	1.593	825	1.422	834	1.761	849	1.587

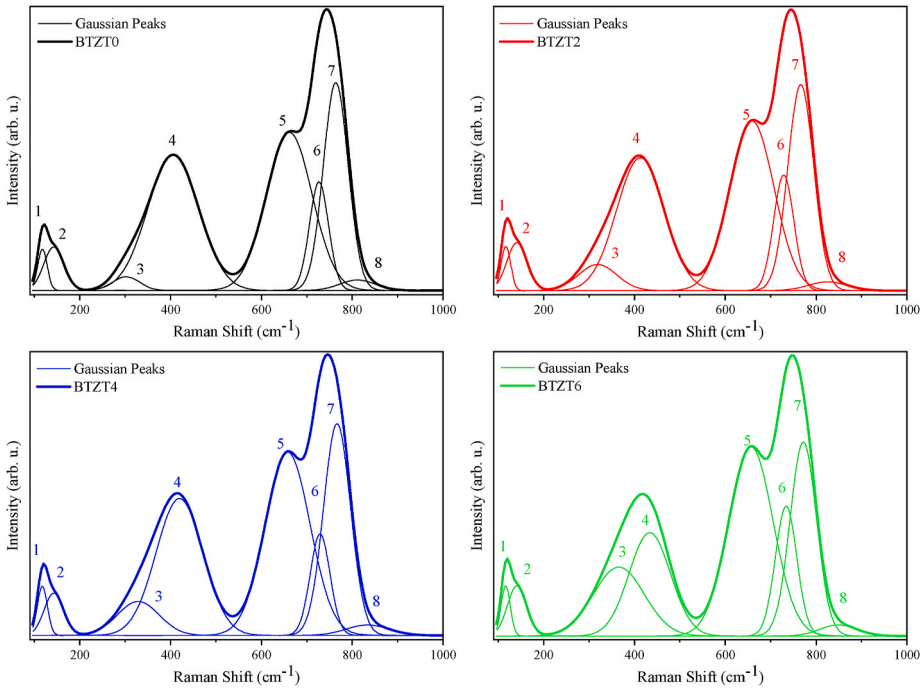


Fig. 5. Raman spectra deconvolutions and Gaussian bands of BTZT glasses.

406–434 cm^{-1} (#4) are associated with the symmetrical stretching or bending vibrations of Te–O–Te linkages that are formed by corner-sharing of (TeO_4), (TeO_{3+1}) polyhedra, and TeO_3 units [26,38]. Gaussian peaks determined in this range shift to a higher wavenumber due to doping with Ta_2O_5. These bonds were decreased in the structure due to the decreasing extent of areas resulting from these bonds' deconvolution process. In addition, Te–O–Bi linkages formation can also be mentioned within this range [39].

Peaks found within the range of 657–661 cm^{-1} (#5) were associated with the axial symmetrical stretching vibrational modes of $(Te_{ax}–O)_s$ of TeO_4 tetrahedra [40]. In addition, when the areas under the Gaussian curves resulting from the deconvolution process were considered, Ta_2O_5 doping shifted the wavenumber to lower values, and these bonds were observed to increase with an increased amount of doping.

According to the literature search, the bands found in the range of 700–800 cm^{-1} (#6 and #7) can be said to be associated with the ZnO_4 tetrahedra [41]. In contrast, the bands observed between 764 and 772 cm^{-1} (#7) were also due to the stretching vibration between Te and non-bridging oxygen (NBO) [42]. This region was seen to shift to a higher wavenumber as a result of Ta_2O_5 doping.

Two different situations are in question in the band formation within the range of 812–849 cm^{-1} (#8). First of all, the band found in this range can be associated with the formation of the stretching vibrations of the TeO_3 trigonal pyramid (tp) units [43]. Except for the BTZT0 sample, this region is also known to belong to Ta–O–Ta vibrational mode [44]. Furthermore, this band was seen to shift to higher wavenumbers with Ta_2O_5 doping.

3.3. Radiation shielding parameters

The linear attenuation coefficient (LAC) of the synthesized BTZT glass system was calculated through three different methods; theoretically via XCOM software [45] and Phy-X/PSD program [46] and simulation via MCNP-5 code [47] in the energy range between 0.015 and 15 MeV. The dependence of the obtained LAC values on both photon energy and Ta_2O_5 content is displayed in Fig. 6. These figures showed that two critical factors affect the LAC values; photon energy and chemical composition of the compounds forming the glass system. According to photon energy, it is more obvious that the LAC decreased sharply with the increase in photon energy. This behavior is attributed and associated with the interaction mechanism of the incident photon with BTZT glasses through the three well-known processes; photoelectric (PE), Compton scattering (CS), and pair production (PP). Due to the dominance of photoelectric (PE) in the low energy zone and the inverse relation of its cross-section with $E^{3.5}$, one found that LAC possesses the maximum values and tends to decreased very sharp. Besides, the

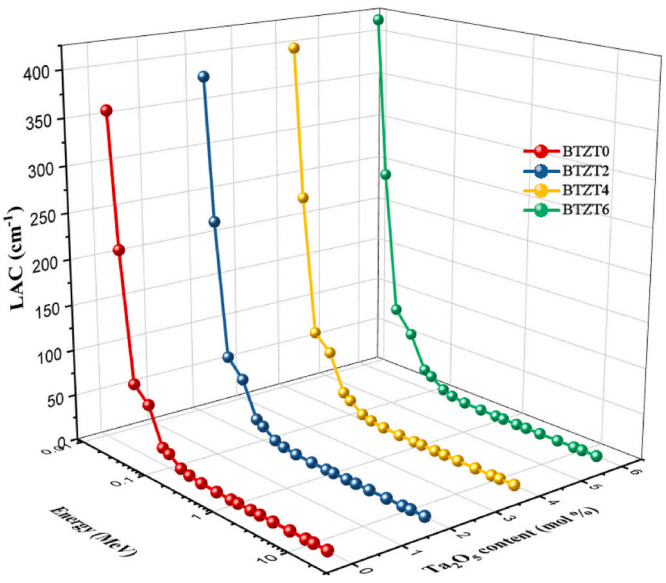


Fig. 6. Variation of linear attenuation coefficient of BTZT glasses with photon energy and Ta_2O_5 content.

cross-section of Compton scattering (CS) is dominant in the intermediate zone and varied as E^{-1}, so a slight change in LAC with photon energy was noticed. Finally, pair production (PP) interactions are dominant at very high photon energy, and then one noticed an increase in the LAC again.

Simulated data presented in Table 3 for LAC showed a change from 373.83 to 431.54 cm^{-1} at the lowest energy range 0.015 MeV, while at the highest energy range; at 15 MeV, LAC varied from 0.257 to 0.274 cm^{-1} for BTZT0 and BTZT6, respectively. The increase in LAC reflects its dependence on the chemical composition of the oxides forming the glass system. For the BTZT glasses, the ZnO (10–4 mol%) is substituted with Ta_2O_5 (0–6 mol%). The mentioned substitution caused an increase in the sample density from 6.216 to 6.465 g cm^{3}and also in the molecular weight from 81.38 to 441.893 g mol^{-1}. Furthermore, the fraction abundance of Ta (Z = 73) increased from 0 to 0.110659, while for Zn (Z = 30), the fractional abundance decreased from 0.035847 to 0.046649 causes an increase in the LAC values. Sample code, chemical composition, and Wt. fraction of elements for $70TeO_2$–$10Bi_2O_3$-(20-x) ZnO-xTa_2O_5 glasses is presented in Table 1. To this end, the synthesized BTZT glasses are arranged in order BTZT6 > BTZT4 > BTZT2 > BTZT0 concerning LAC values.

Fig. 7 introduced a correlation between the simulated MCNP-5 (LAC, cm^{-1}) and theoretical XCOM (LAC, cm^{-1}) for BTZT0 and BTZT6, which showed that the R square approximately equal one, which appeared the excellent matching with high accuracy between the two methods of calculations. The LAC also calculated using the Phy-X/PSD program in the studied energy range [43]. The results obtained utilizing the Phy-X program were compared to those simulated using the MCNP-5 code and XCOM software database, as illustrated in Table 3. The difference between the MCNP-5 and XCOM was calculated and coded Δ_1 (%), while

Table 3
The linear attenuation coefficient and diff (%) between the MCNP-5 and XCOM data.

Energy (MeV)	linear attenuation coefficient LAC (cm^{-1})									
	BTZT0					BTZT2				
	MCNP-5	XCOM	Phy-X/PSD	Δ_1 (%)	Δ_2 (%)	MCNP-5	XCOM	Phy-X/PSD	Δ_1 (%)	Δ_2 (%)
0.015	359.3890	361.8955	361.8720	−0.6974	−0.6909	380.4306	380.8036	380.8088	−0.0980	−0.0994
0.02	215.3084	218.1816	218.1557	−1.3344	−1.3224	225.1593	225.8919	225.8824	−0.3254	−0.3211
0.03	74.1510	75.4001	75.3928	−1.6845	−1.6748	77.6156	78.0845	78.0964	−0.6041	−0.6194
0.15	5.9186	5.4253	5.4254	8.3337	8.3326	6.1908	5.6420	5.6417	8.8655	8.8698
0.2	3.0154	2.8351	2.8353	5.9790	5.9736	3.1360	2.9392	2.9392	6.2757	6.2741
0.3	1.3272	1.3190	1.3191	0.6133	0.6060	1.3745	1.3586	1.3586	1.1536	1.1525
0.5	0.6695	0.6744	0.6743	−0.7405	−0.7203	0.6859	0.6884	0.6886	−0.3726	−0.3931
0.8	0.4459	0.4482	0.4482	−0.5214	−0.5222	0.4537	0.4554	0.4554	−0.3630	−0.3691
1	0.3728	0.3827	0.3827	−2.6362	−2.6375	0.3784	0.3882	0.3882	−2.5955	−2.5901
1.5	0.2950	0.2997	0.2998	−1.6193	−1.6268	0.2989	0.3037	0.3037	−1.6112	−1.6037
2	0.2610	0.2639	0.2639	−1.1094	−1.1064	0.2646	0.2674	0.2674	−1.0719	−1.0679
3	0.2320	0.2337	0.2337	−0.7457	−0.7351	0.2355	0.2371	0.2371	−0.6653	−0.6582
5	0.2194	0.2204	0.2204	−0.4627	−0.4582	0.2233	0.2240	0.2240	−0.3143	−0.3240
8	0.2262	0.2271	0.2271	−0.3742	−0.3765	0.2308	0.2312	0.2312	−0.2061	−0.1928
10	0.2349	0.2357	0.2357	−0.3562	−0.3560	0.2398	0.2402	0.2402	−0.1505	−0.1518
15	0.2576	0.2585	0.2585	−0.3614	−0.3493	0.2634	0.2637	0.2637	−0.1075	−0.1119
Energy (MeV)	linear attenuation coefficient LAC (cm^{-1})									
	BTZT4					BTZT6				
	MCNP-5	XCOM	Phy-X/PSD	Δ_1 (%)	Δ_2 (%)	MCNP-5	XCOM	Phy-X/PSD	Δ_1 (%)	Δ_2 (%)
0.015	398.4064	398.9018	398.9205	−0.1243	−0.1290	418.1651	418.8027	418.8082	−0.0013	−0.1538
0.02	232.6014	233.3019	233.3027	−0.3012	−0.3015	241.2138	241.9203	241.9025	−0.3254	−0.2855
0.03	80.2182	80.6703	80.6924	−0.5636	−0.5911	83.2224	83.7218	83.6950	−0.6041	−0.5679
0.15	6.3849	5.8491	5.8491	8.3918	8.3911	6.3513	6.0849	6.0852	8.8655	4.1905
0.2	3.2351	3.0393	3.0390	6.0528	6.0615	3.2049	3.1543	3.1540	6.2757	1.5893
0.3	1.4426	1.3966	1.3967	3.1882	3.1863	1.4539	1.4423	1.4420	1.1536	0.8136
0.5	0.6996	0.7024	0.7024	−0.4080	−0.3989	0.7173	0.7202	0.7201	−0.3726	−0.4008
0.8	0.4607	0.4623	0.4624	−0.3658	−0.3720	0.4703	0.4720	0.4720	−0.3630	−0.3775
1	0.3835	0.3936	0.3936	−2.6378	−2.6364	0.3909	0.4013	0.4013	−2.5955	−2.6796
1.5	0.3026	0.3076	0.3076	−1.6212	−1.6280	0.3082	0.3132	0.3133	−1.6112	−1.6557
2	0.2679	0.2708	0.2708	−1.0792	−1.0839	0.2729	0.2759	0.2759	−1.0719	−1.0989
3	0.2388	0.2404	0.2404	−0.6644	−0.6656	0.2434	0.2451	0.2451	−0.6653	−0.6723
5	0.2268	0.2276	0.2276	−0.3380	−0.3259	0.2316	0.2324	0.2324	−0.3143	−0.3267
8	0.2348	0.2352	0.2352	−0.1873	−0.1915	0.2401	0.2406	0.2406	−0.2061	−0.1924
10	0.2441	0.2445	0.2445	−0.1481	−0.1493	0.2498	0.2502	0.2502	−0.1505	−0.1487
15	0.2684	0.2687	0.2687	−0.1054	−0.1113	0.2750	0.2753	0.2753	−0.1075	−0.1106

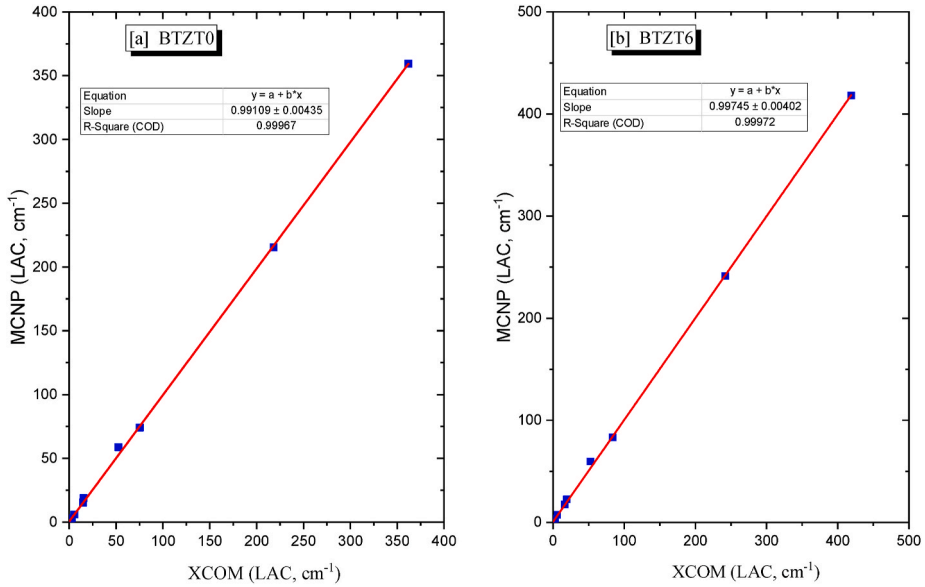


Fig. 7. Correlation between the Monte Carlo and theoretical LAC for BTZT0 and BTZT4.

the difference between the MCNP-5 code and the Phy-X program was coded Δ_2 (%). The values of Δ_1 and Δ_2 were calculated according to equations (4 and 5).

$$\Delta_1(\%) = \frac{[(LAC)_{MCNP} - (LAC)_{XCOM}]^*100}{(LAC)_{MCNP}} \quad (4)$$

$$\Delta_2(\%) = \frac{[(LAC)_{MCNP} - ((LAC)_{Phy-X/PSD})]^*100}{(LAC)_{MCNP}} \quad (5)$$

the calculated values of Δ_1 and Δ_2 are closed together and were found to be less than 8%. The matching between Δ_1 and Δ_2 is due to the fact that the Phy-X/PSD is similar to XCOM software; they use the NIST database to evaluate the shielding parameters of any shielding material.

Based on the LAC, one has calculated the half-value layer (HVL) of the prepared BTZT glasses. The variation of the half-value layer of BTZT glasses with photon energy in the selected range is displayed in Fig. 8. From this figure, one can see that the HVL exhibits an inverse trend with which obtained in LAC; HVL has the smallest values in photoelectric low energy zone and increased in the intermediate and high energy zone; zones of CS and PP dominance. Furthermore, the increase in the Ta_2O_5 molar content decreased the HVL gradually. BTZT0 has the maximum HVL and ranged from 0.00185 to 2.694 cm, where regarding BTZT6, the HVL found ranged from 0.00161 to 2.525 cm at 0.015 and 15 MeV, respectively.

The sample density's importance is more apparent when one studies the relation of HVL with sample density at different photon energy, as is displayed in Fig. 9. From this figure, one noticed that the more the density increased, the more the samples' shielding effect was enhanced through the decrease in the HVL. Besides, the HVL increased with the increase in the photon energy from 0.015 to 15 MeV. Figs. 8 and 9 showed that the BTZT6 glass samples are promising gamma shields among all fabricated glasses.

The transmission factor TF (%) was calculated for the fabricated BTZT glass samples at some fixed energies 0.5, 1, 5, and 10 MeV. Fig. 10 exhibits that the TF variation is related to three different factors. The first is the gamma photon energy, where the TF factor increased with

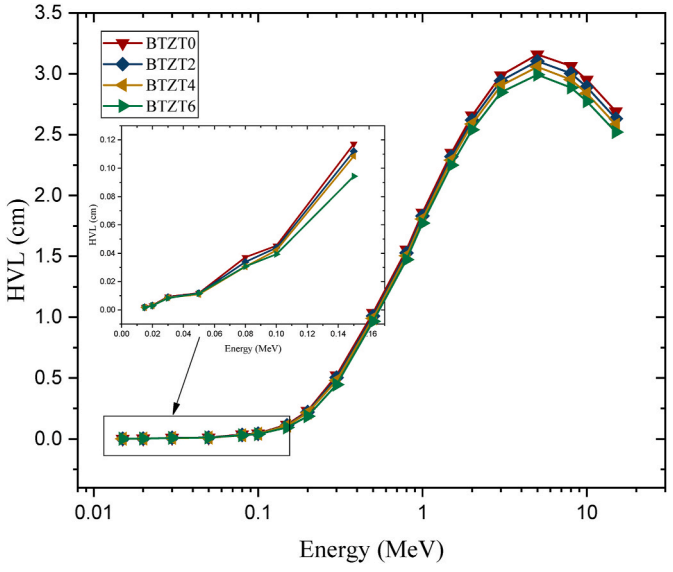


Fig. 8. Variation of half value layer of BTZT glasses with photon energy.

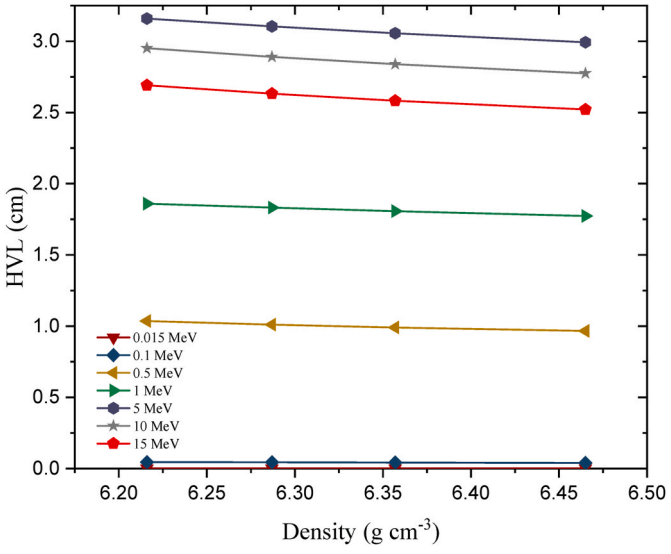


Fig. 9. Dependence of half value layer of BTZT glasses on the samples density at definite photon energy.

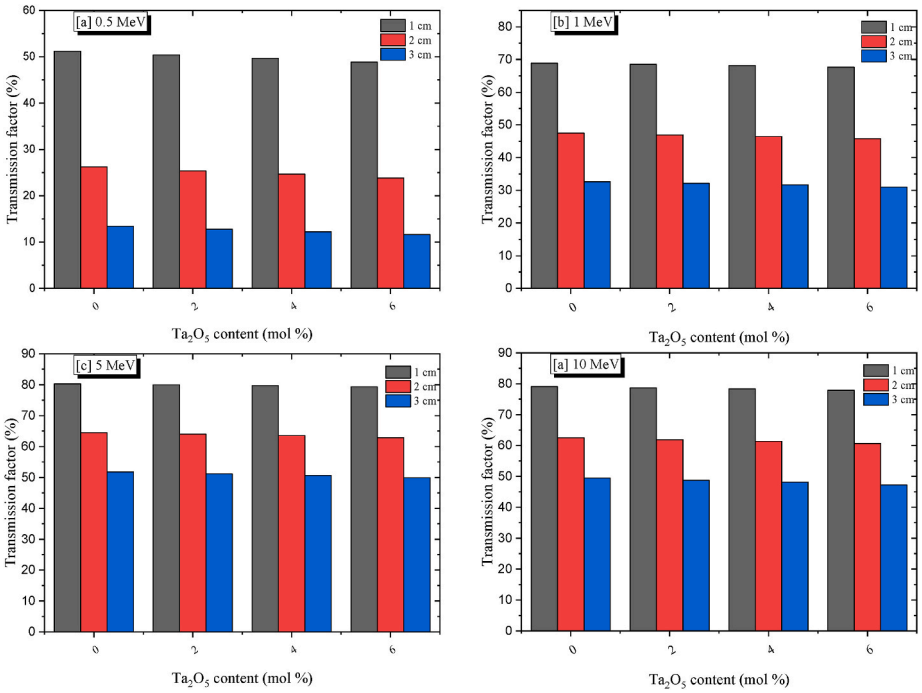


Fig. 10. Dependence of the transmission factor on the glass thickness different photon energy.

increasing the Photon-energy. The lowest TF obtained at the lower photon energies for 0.5 MeV, as shown in subfigure Fig. 10a. The mentioned subfigure presents that the glasses thickness of 3 cm can absorb or shield around 88.373% for the glass with 6 mol% of the Ta_2O_5 contents. In contrast, the highest TF received at higher gamma photon energies around 10 MeV, as illustrated in subfigure 10 d. A glass with the same thickness (i.e., 3 cm) can only shield about 52.741% for the glass sample with 6 mol% of the Ta_2O_5 content at the mentioned energy. Increasing the incoming photon energy was associated with increasing the incoming photons' mass stopping power, which caused a rise in the number of transmitted photons. The second factor is the chemical composition of the fabricated BTZT glass samples, where the TF is slowly decreased with increasing the Ta_2O_5 content between 0 and 6 mol%. As illustrated in subfigure, 10b for gamma energy 1 MeV, a glass sample with a thickness of 2 cm can reduce the TF from 47.442 to 45.760%, raising the Ta_2O_5 increases between 0 and 6 mol%, respectively. The Ta_2O_5 addition's effect appears clearly in Fig. 10a–d, where the addition of Ta_2O_5 raises the density and molar weight of the fabricated BTZT glass samples. The dense materials, the better LAC achieved for the fabricated glasses, as we know. Thus, the glass sample without Ta_2O_5 (i.e., BTZT0) has a lower LAC than the glass sample with 6 mol % of the Ta_2O_5 (i.e., BTZT6). The TF received from BTZT0 will be higher than that obtained from BTZT6 at any photon energy. The third factor is the material thickness, where the transmission of gamma photons is positively affected by the shielding thickness. The TF is strongly decreased with a growth in the glass thickness. Subfigure 10c depicts that the TF reduced from 80.299 to 52.77% (for glass BTZT0) and 79.706 to 47.259% (for glass coded BTZT4) with increasing the glass thickness between 1 and 3 cm, respectively. The time needed for the gamma photons to penetrate thicker thicknesses is higher than that required for the thinner thicknesses for a given material. Thus, the photons will make many collisions with the glass atoms a long it tracks length, and almost all of the incoming photons will be absorbed or scattered inside the glass thickness. This will cause higher attenuation and lower TF.

4. Conclusion

A new glass series consists of four samples doped with various ratios of Ta_2O_5 was prepared according to the formula $10Bi_2O_3$–$70TeO_2$-·(20-x)ZnO-·xTa_2O_5; where, x = 0, 2, 4, 6 mol%. The fabricated BTZT glass samples' density was observed to vary between 6.216 and 6.465 g cm^{-3}, with an increase in the Ta_2O_5 content between 0 and 6 mol%, respectively. Simultaneously, the fabricated glass samples' molar volume was ranged between 28.0875 and 30.3516 cm^3 mol^{-1}. The XRD spectrometer was used to confirm the amorphous phase, and the Renishaw Invia Raman microscope spectrometer was used to characterize the fabricated glass samples' structure. Moreover, the Monte Carlo simulation MCNP-5 code and XCOM software program were utilized to evaluate LAC's fabricated glass samples. The obtained results depict that at photon energy 0.015 MeV, the LAC reaches the maximum, varied between 359.389 and 418.165 cm^{-1}. In contrast, the lowest LAC was calculated at 15 MeV and changed between 0.257 and 0.275 cm^{-1}, increasing the Ta_2O_5 doping ratio between 0 and 6 mol%. The HVL was found to grow from 0.001 to 2.690 cm and from 0.001 to 2.520 cm for glass samples BTZT0 and BTZT6, respectively. The TF was also found to decrease with an increase in the Ta_2O_5 doping ratio.

CRediT authorship contribution statement

Gokhan Kilic: Conceptualization, Methodology, Software, Writing - review & editing. **F.I.El-Agawany:** Data curation, Writing - original draft, Writing - review & editing. **Buse Ozen Ilik:** Visualization, Investigation. **K.A.Mahmoud:** Data curation, Writing - original draft, Software, Validation. **Erkan Ilik:** Visualization, Investigation. **Y.S. Rammah:** Supervision, Writing - review & editing.

Declaration of competing interest

The authors declare that they have no known competing financial interests or personal relationships that could have appeared to influence the work reported in this paper.

Appendix A. Supplementary data

Supplementary data to this article can be found online at https://doi.org/10.1016/j.optmat.2020.110757.

References

[1] M.S. Al-Buriahi, F.I. El-Agawany, C. Sriwunkum, H. Akyıldırım, H. Arslan, B. T. Tonguc, R. El-Mallawany, Y.S. Rammah, Influence of Bi_2O_3/PbO on nuclear shielding characteristics of lead-zinc-tellurite glasses, Phys. B Condens. Matter 581 (2020) 411946.

[2] H.O. Tekin, V.P. Singh, E.E. Altunsoy, M. Karahan, M.I. Sayyed, T.T. Erguzel, E. S. Kasikci, M. Konuk, Gamma shielding properties of erbium zinc tellurite glass system using Monte Carlo method, J. Test. Eval. 48 (2020) 1252–1261.

[3] H.O. Tekin, M.I. Sayyed, T. Manici, E.E. Altunsoy, Photon shielding characterizations of bismuth modified borate–silicate–tellurite glasses using MCNPX Monte Carlo code, Mater. Chem. Phys. 211 (2018) 9–16.

[4] G. Kilic, U.G. Issever, E. Ilik, The synthesis and characterization of zinc-tellurite semiconducting oxide glasses containing Ta_2O_5, Mater. Res. Express 6 (2019), 065907.

[5] B. Eraiah, Optical properties of samarium doped zinc-tellurite glasses, Bull. Mater. Sci. 29 (2006) 375–378.

[6] X.J. Shen, Y.R. Zhu, Z.Z. Zhou, X.E. Su, M.H. Zhou, Y.X. Zhou, Pr^{3+}/Nd^{3+} codoped tellurite glass for O+E+S-band broad emission, Optoelectron. Lett. 15 (2019) 424–427.

[7] S.G. Upender, V. Sreenivasulu, M. Prasad, Spectroscopic and Optical Properties of the VO_2+ ion doped TeO_2-TiO_2-ZnO-Nb_2O_5 glass system, Journal of Korean Physics Society 68 (2016) L998–L1007.

[8] M.R. Sahar, Glass-formation in the TeO_2-ZnO-$PbCl_2$ system, J. Mater. Sci. Lett. 13 (1994) 1640–1641.

[9] M.R. Sahar, K. Sulhadi, M.S. Rohani, Spectroscopic studies of TeO_2-ZnO-Er_2O_3 glass system, J. Mater. Sci. 42 (2007) 824–827.

[10] A.E. Ersundu, M. Büyükyıldız, M.C. Ersundu, E. Şakar, M. Kurudirek, The heavy metal oxide glasses within the WO_3-MoO_3-TeO_2 system to investigate the shielding properties of radiation applications, Prog. Nucl. Energy 104 (2018) 280–287.

[11] M.C. Ersundu, A.E. Ersundu, N. Gedikoğlu, E. Şakar, M. Büyükyıldız, M. Kurudirek, Physical, mechanical and gamma-ray shielding properties of highly transparent ZnO-MoO_3-TeO_2 glasses, J. Non-Cryst. Solids 524 (2019) 119648.

[12] P. Kaur, K.J. Singh, M. Kurudirek, S. Thakur, Study of environment friendly bismuth incorporated lithium borate glass system for structural, gamma-ray and fast neutron shielding properties, Spectrochim. Acta Mol. Biomol. Spectrosc. 223 (2019) 117309.

[13] M.J. Redman, J.H. Chen, Zinc tellurite glasses, J. Am. Ceram. Soc. 50 (1967) 523–525.

[14] N.S. Tagiara, D. Palles, E.D. Simandiras, V. Psycharis, A. Kyritsis, E.I. Kamitsos, Synthesis, thermal and structural properties of pure TeO_2 glass and zinc-tellurite glasses, J. Non-Cryst. Solids 457 (2017) 116–125.

[15] H.A.A. Sidek, S. Rosmawati, Z.A. Talib, M.K. Halimah, W.M. Daud, Synthesis and optical properties of ZnO-TeO_2 glass system, Am. J. Appl. Sci. 6 (2009) 1489–1494.

[16] R. Rajeswari, S.S. Babu, C.K. Jayasankar, Spectroscopic characterization of alkali modified zinc-tellurite glasses doped with neodymium, Spectrochim. Acta Mol. Biomol. Spectrosc. 77 (2010) 135–140.

[17] K. Aishwarya, G. Vinitha, G.S. Varma, S. Asokan, N. Manikandan, Synthesis and characterization of barium fluoride substituted zinc tellurite glasses, Phys. B Condens. Matter 526 (2017) 84–88.

[18] M.I. Sayyed, Bismuth modified shielding properties of zinc boro-tellurite glasses, J. Alloys Compd. 688 (2016) 111–117.

[19] I.-I. Oprea, H. Hesse, K. Betzler, Optical properties of bismuth borate glasses, Opt. Mater. 26 (2004) 235–237.

[20] M. Dult, R.S. Kundu, S. Murugavel, R. Punia, N. Kishore, Conduction mechanism in bismuth silicate glasses containing titanium, Phys. B Condens. Matter 452 (2014) 102–107.

[21] L. Dimesso, G. Gnappi, A. Montenero, P. Fabeni, G.P. Pazzi, The crystallization behaviour of bismuth germanate glasses, J. Mater. Sci. 26 (1991) 4215–4219.

[22] T.Z. Babeva, E. Atanassova, J. Koprinarova, Optical characteristics of thin rf sputtered Ta_2O_5 layers, Phys. Status Solidi 202 (2005) 330–336.

[23] S. Satoh, K. Susa, I. Matsuyama, Sol–gel preparation and optical properties of SiO_2–Ta_2O_5 glass, J. Non-Cryst. Solids 306 (2002) 300–308.

[24] G.S. Murugan, Y. Ohishi, Structural and physical properties of a novel TeO_2–BaO–SrO–Ta_2O_5 glass system for photonic device applications, J. Non-Cryst. Solids 351 (2005) 364–371.

[25] G. Kilic, U.G. Issever, E. Ilik, Characterization of Er^{3+} doped ZnTeTa semiconducting oxide glass, J. Mater. Sci. Mater. Electron. 30 (2019) 8920–8930.

[26] G. Kilic, U.G. Issever, E. Ilik, Synthesis, characterization and crystalline phase studies of TeO_2-Ta_2O_5-ZnO/ZnF_2 oxyfluoride semiconducting glasses, J. Non-Cryst. Solids 527 (2020) 119747.

[27] M.S. Al-Buriahi, Y.S. Rammah, Electronic polarizability, dielectric, and gamma-ray shielding properties of some tellurite-based glasses, Appl. Phys. A 125 (2019) 678.

[28] Y.S. Rammah, K.A. Mahmoud, E. Kavaz, Ashok Kumar, F.I. El-Agawany, The role of PbO/Bi_2O_3 insertion on the shielding characteristics of novel borate glasses, Ceram. Int. 46 (2020) 23357–23368.

[29] F.I. El-Agawany, O.L. Tashlykov, K.A. Mahmoud, Y.S. Rammah, The radiation-shielding properties of ternary SiO_2–SnO–SnF_2 glasses: simulation and theoretical study, Ceram. Int. 46 (15) (2020) 23369–23378.

[30] A.M. Ali, Y.S. Rammah, M.I. Sayyed, H.H. Somaily, H. Algarni, M. Rashad, The impact of lead oxide on the optical and gamma shielding properties of barium borate glasses, Appl. Phys. A 126 (2020) 280.

[31] A. Alalawi, M.S. Al-Buriahi, Y.S. Rammah, Radiation shielding properties of PNCKM bioactive glasses at nuclear medicine energies, Ceram. Int. 46 (10) (2020) 15027–15033.

[32] G. Kilic, E. Ilik, U.G. Issever, M. Peker, The effect of B_2O_3/CdO substitution on structural, thermal, and optical properties of new black PVB/Cd semiconducting oxide glasses, Appl. Phys. A 126 (2020) 1–12.

[33] G. Kilic, Role of Nd^{3+} ions in TeO_2–V_2O_5–(B_2O_3/Nd_2O_3) glasses: structural, optical, and thermal characterization, J. Mater. Sci. Mater. Electron. 31 (2020) 12892–12902.

[34] A. Chagraoui, A. Chakib, A. Mandil, A. Tairi, Z. Ramzi, S. Benmokhtar, New investigation within ZnO–TeO_2–Bi_2O_3 system in air, Scripta Mater. 56 (2007) 93–96.

[35] J. Ozdanova, H. Ticha, L. Tichy, Remark on the optical gap in ZnO–Bi_2O_3–TeO_2 glasses, J. Non-Cryst. Solids 353 (2007) 2799–2802.

[36] E. Mendoza-Mendoza, A.G. Nuñez-Briones, R. Leyva-Ramos, R.D. Peralta-Rodríguez, L.A. García-Cerda, E.D. Barriga-Castro, R. Ocampo-Pérez, J. Rodríguez-Hernández, A novel two-step route for synthesizing pure Ta_2O_5 nanoparticles with enhanced photocatalytic activity, Ceram. Int. 45 (2019) 6268–6274.

[37] L. Kumari, J.-H. Lin, Y.-R. Ma, One-dimensional Bi_2O_3 nanohooks: synthesis, characterization and optical properties, J. Phys. Condens. Matter 19 (40) (2007) 406204.

[38] V. Sreenivasulu, G. Upender, V.V. Priya, V.C. Mouli, M. Prasad, D.S.C. Raman, ESR and optical properties of lithium cadmium zinc tellurite glasses, Phys. B Condens. Matter 454 (2014) 60–66.

[39] M. Udovic, P. Thomas, A. Mirgorodsky, O. Durand, M. Soulis, O. Masson, T. Merle-Méjean, J.-C. Champarnaud-Mesjard, Thermal characteristics, Raman spectra and structural properties of new tellurite glasses within the Bi_2O_3–TiO_2–TeO_2 system, J. Solid State Chem. 179 (2006) 3252–3259.

[40] T. Sekiya, N. Mochida, A. Soejima, Raman spectra of binary tellurite glasses containing tri-or tetra-valent cations, J. Non-Cryst. Solids 191 (1995) 115–123.

[41] L.-G. Hwa, S.-L. Hwang, L.-C. Liu, Infrared and Raman spectra of calcium alumino–silicate glasses, J. Non-Cryst. Solids 238 (1998) 193–197.

[42] A.K. Yadav, P. Singh, A review of the structures of oxide glasses by Raman spectroscopy, RSC Adv. 5 (2015) 67583–67609.

[43] G.S. Murugan, Y. Ohishi, TeO_2–BaO–SrO–Nb_2O_5 glasses: a new glass system for waveguide devices applications, J. Non-Cryst. Solids 341 (2004) 86–92.

[44] P. Sudhakar, A.S.S. Reddy, Y. Zhydachevskyy, A. Suchocki, M.G. Brik, V.R. Kumar, M. Piasecki, N. Veeraiah, Luminescence characteristics of Er^{3+} ions in ZnO-Ta_2O_5/Nb_2O_5/ZrO_2-B_2O_3 glass system-A case study of energy transfer from ZnO to Er^{3+} ions, Opt. Mater. 86 (2018) 87–94.

[45] M.J. Berger, j H. Hubbel, S.M. Seltzer, J. Chang, J.S. Coursey, R. Sukumar, D. S. Zucker, XCOM: Photon Cross Sections Database, 2010, https://doi.org/10.18434/T48G6X.

[46] Ş. Erdem, F. Özgür, B. Al, M.I. Sayyed, M. Kurudirek, Phy-X/PSD : development of a user friendly online software for calculation of parameters relevant to radiation shielding and.

[47] X-5 Monte Carlo Team, MCNP-A General Monte Carlo N-Particle Transport Code, Version 5, Los Alamos Controlled Publication. LA-CP-03-0245, 2003.